Astron. Astrophys. 355, 900–914 (2000)

ASTRONOMY AND ASTROPHYSICS

The Fornax spectroscopic survey

I. Survey strategy and preliminary results on the redshift distribution of a complete sample of stars and galaxies

M.J. Drinkwater[1], **S. Phillipps**[2], **J.B. Jones**[2], **M.D. Gregg**[3], **J.H. Deady**[2], **J.I. Davies**[4], **Q.A. Parker**[5], **E.M. Sadler**[6], **and R.M. Smith**[4]

[1] School of Physics, University of Melbourne, Parkville, Victoria 3010, Australia
[2] Department of Physics, University of Bristol, Tyndall Avenue, Bristol, BS8 1TL, England, UK
[3] University of California, Davis, and Institute for Geophysics and Planetary Physics, Lawrence Livermore National Laboratory, L-413, Livermore, CA 94550, USA
[4] Department of Physics and Astronomy, University of Wales Cardiff, P.O. Box 913, Cardiff, CF2 3YB, Wales, UK
[5] Royal Observatory Edinburgh, Blackford Hill, Edinburgh, EH9 3HJ, Scotland, UK
[6] School of Physics, University of Sydney, NSW 2006, Australia

Received 11 October 1999 / Accepted 25 January 2000

Abstract. The *Fornax Spectroscopic Survey* will use the Two degree Field spectrograph (2dF) of the Anglo-Australian Telescope to obtain spectra for a complete sample of all 14000 objects with $16.5 \leq b_j \leq 19.7$ in a 12 square degree area centred on the Fornax Cluster. The aims of this project include the study of dwarf galaxies in the cluster (both known low surface brightness objects and putative normal surface brightness dwarfs) and a comparison sample of background field galaxies. We will also measure quasars and other active galaxies, any previously unrecognised compact galaxies and a large sample of Galactic stars. By selecting all objects—both stars and galaxies—independent of morphology, we cover a much larger range of surface brightness and scale size than previous surveys.

In this paper we first describe the design of the survey. Our targets are selected from UK Schmidt Telescope sky survey plates digitised by the Automated Plate Measuring (APM) facility. We then describe the photometric and astrometric calibration of these data and show that the APM astrometry is accurate enough for use with the 2dF. We also describe a general approach to object identification using cross-correlations which allows us to identify and classify both stellar and galaxy spectra.

We present results from the first 2dF field. Redshift distributions and velocity structures are shown for all observed objects in the direction of Fornax, including Galactic stars, galaxies in and around the Fornax Cluster, and for the background galaxy population. The velocity data for the stars show the contributions from the different Galactic components, plus a small tail to high velocities. We find no galaxies in the foreground to the cluster in our 2dF field. The Fornax Cluster is clearly defined kinematically. The mean velocity from the 26 cluster members having reliable redshifts is $1560 \pm 80\,\mathrm{km\,s^{-1}}$. They show a velocity dispersion of $380 \pm 50\,\mathrm{km\,s^{-1}}$. Large-scale structure can be traced behind the cluster to a redshift beyond $z = 0.3$. Background compact galaxies and low surface brightness galaxies are found to follow the general galaxy distribution.

Key words: astrometry – galaxies: active – galaxies: statistics – stars: statistics – surveys – techniques: spectroscopic

Send offprint requests to: M.J. Drinkwater

1. Introduction

The development of a new generation of multi-object spectrographs, exemplified by the 'Two degree Field', or 2dF, multi-fibre spectrograph on the Anglo-Australian Telescope (AAT), has opened up whole new areas of astronomical survey science. One particular area, which we discuss in this paper, is the opportunity to make a truly complete spectroscopic survey of a given area on the sky, down to well determined, faint limits, irrespective of image morphology or any other preselection of target type.

The *Fornax Spectroscopic Survey*, or FSS, seeks to exploit the huge multiplexing advantage of 2dF by surveying a region of 12 square degrees centred on the Fornax Cluster of galaxies. It will encompass both cluster galaxies, of a wide range of types and magnitudes, and background and foreground galaxies (over a similarly wide range of morphologies), as well as Galactic stars, QSOs and any unusual or rare objects.

Although many surveys of nearby clusters have been made over the past 20 years or more, these are all limited in several crucial aspects. Spectroscopic surveys exist, but typically only of the few dozen brightest cluster galaxies (and any background interlopers in the top few magnitudes of the cluster luminosity function). Photometric surveys, of course, go much deeper, but such studies must be of a statistical nature (e.g. subtracting off the expected background numbers; Smith et al. 1997), or rely on subjective judgements of likely cluster membership based on morphology, surface brightness or colour (e.g. Ferguson 1989). Of particular concern is the surface brightness;

low surface brightness galaxies (LSBGs) seen towards a cluster are conventionally assumed to be members, while apparently faint, but high surface brightness galaxies (HSBGs) are presumed to be luminous objects in the background (e.g. Sandage et al. 1985). The failure of either assumption, i.e. the existence of large background LSBGs (such as the serendipitously discovered Malin 1; Bothun et al. 1987) or of a population of high surface brightness (compact) dwarfs in the cluster (Drinkwater & Gregg 1998), can have a dramatic effect on our perception of the galaxy population as a whole. Furthermore, it is possible that a population of extremely compact galaxies (either in the cluster or beyond) could masquerade as stars and hence be missed altogether from galaxy samples. Examples have previously been found in, for example, QSO surveys, but again these are serendipitous discoveries and hard to quantify (see Drinkwater et al. 1999a = Paper II, and references therein).

Few previous attempts at all-object surveys have been made. The one most similar to ours is probably that of Morton and Tritton in the early 1980s. They obtained around 600 objective prism spectra and 100 slit spectra for objects in a 0.31 square degree region of background sky (i.e. no prominent cluster) over the course of a 5 year period (Morton et al. 1985). More recently Colless et al. (1993) obtained spectra of about 100 objects in a small area of sky and small magnitude range in order to investigate the completeness of faint galaxy redshift surveys.

Our overall survey will therefore represent a huge increase in the volume of data and in addition will give a uniquely complete picture of a cluster of galaxies. It is worth noting that the huge galaxy surveys planned, with 2dF (Folkes et al. 1999; Colless 1999) or the Sloan Digital Survey (Gunn 1995; Loveday & Pier 1998) will not address such problems, since their galaxy samples will be pre-selected from photometric surveys and will only include objects classified as galaxies and not of too low surface brightness, thus removing both ends of any potentially wide range of galaxy parameters.

In the present paper we discuss the design and aims of our all-object *Fornax Spectroscopic Survey* (FSS) and present initial results on the velocity distributions. Sect. 2 gives a technical definition of the survey, describing the relevant features of the 2dF spectrograph, the selection of our target catalogue and the calibration of this input catalogue. In Sect. 3 we discuss the scientific aims of the survey and summarise the types and numbers of objects we expect to observe. In Sect. 4 we discuss the spectroscopic observations and observational strategy. We describe the technique we have developed to identify and classify objects automatically from the 2dF spectra and give some examples from our initial observations. Sect. 5 gives the initial redshift results and Sect. 6 summarises the survey work to date.

2. The survey design

In this section we describe the basic parameters of the FSS. We start with the relevant technical details of the 2dF spectrograph, and then discuss our selection of targets from the digitised photographic sky survey plates and the calibration of our input catalogues.

2.1. The 2dF spectrograph

The 2dF facility (Taylor et al. 1998) is probably the most complex ground-based astronomical instrument built to date. Via a straightforward 'top-end' change the capability of the 3.9-m Anglo-Australian Telescope is transformed into an unique wide-field multi-fibre spectroscopic survey instrument. Up to 400 fibres are available at any one time for rapid configuration over the full two-degree diameter focal surface via a highly accurate robotic positioner mounted in situ. Each 2 arcsec diameter fibre can be placed to an accuracy of 0.3 arcsec in less than 10 seconds. The input target positions must be accurate to 0.3 arcsec r.m.s. or better over the whole two-degree field to avoid vignetting of the fibre entrance apertures. This requirement is only for relative positions; the absolute accuracy of a complete set of targets and guide stars need only be $1-2$ arcsec as the guide stars will then centre all the targets accurately.

The wide field is provided by a highly sophisticated multi-component corrector with in-built atmospheric dispersion compensator. In a novel arrangement 2dF can simultaneously observe 400 target objects on the sky at the same time that a further 400 fibres are being configured using the robotic positioner on one of the two available 'field plates' (focal surfaces). Once observations and configurations have been completed (usually over the same timescale) a tumbling mechanism allows the newly configured field plate to point at the sky whilst the previously observed field can be re-configured for the next target field. In this way rapid field inter-change is provided for an extremely efficient observing environment. Each set of 400 fibres feeds two spectrographs which accept 200 fibres each. These are mounted on the 2dF top end ring and can produce low to medium resolution spectra on the dedicated 1024×1024 TEK CCDs.

The 2dF is now operating at close to the original specifications anticipated for this most complex of instruments (Lewis et al. 1998). Field configuration times of about 1 hour for 400 fibres permit rapid cycling of target fields and have enabled excellent progress to be made with our complete survey.

2.2. The Fornax Cluster field

We chose the Fornax Cluster for this study because it is a well-studied, compact, nearby southern galaxy cluster suited to this type of survey. We and several other groups have made photometric or small-scale spectroscopic surveys of the region (e.g. Ferguson 1989; Davies et al. 1988; Drinkwater & Gregg 1998; Hilker et al. 1999). The published spectroscopic samples have either been very small or have concentrated on the brighter cluster galaxies (Jones & Jones 1980; Drinkwater et al. 2000a). A search of NED[1] in our central 2dF field (number 1 in Table 1) found only 42 objects brighter than $B = 20$ with measured redshifts: 30 cluster galaxies, 6 background galaxies and 6 QSOs.

[1] The NASA/IPAC Extragalactic Database (NED) is operated by the Jet Propulsion Laboratory, California Institute of Technology, under contract with the National Aeronautics and Space Administration.

Table 1. Fornax Spectroscopic Survey Fields

N	RA (J2000) Dec	*l*, *b*	Comments
1	03 38 29.0 −35 27 01	236.7, −53.6	NGC1399
2	03 28 40.0 −35 27 01	236.8, −55.6	
3	03 33 38.0 −33 41 59	233.7, −54.6	
4	03 43 15.0 −33 41 59	233.8, −52.6	

With 2dF we can now measure the redshifts of some 700–900 galaxies and quasars in this same field.

The Fornax Cluster is concentrated within one United Kingdom Schmidt Telescope (UKST) Sky Survey plate and our survey will comprise four separate 2dF fields which are listed in Table 1. We show the distribution of our fields on the sky in Fig. 1 compared to the positions of galaxies classified as likely cluster members by Ferguson (1989). Our first field is centred on the large galaxy NGC 1399 at the centre of the cluster. In order both to cover a large number of targets and to go significantly deeper than previous spectroscopic surveys we chose to limit our survey at a b_j magnitude of 19.7. This is then essentially the same depth as the large scale 2dF Galaxy Redshift Survey (GRS) of Ellis, Colless and collaborators (e.g. Colless 1999; Folkes et al. 1999). This combination of survey area and magnitude limit will optimise our measurement of the cluster galaxies (see Sect. 3.1).

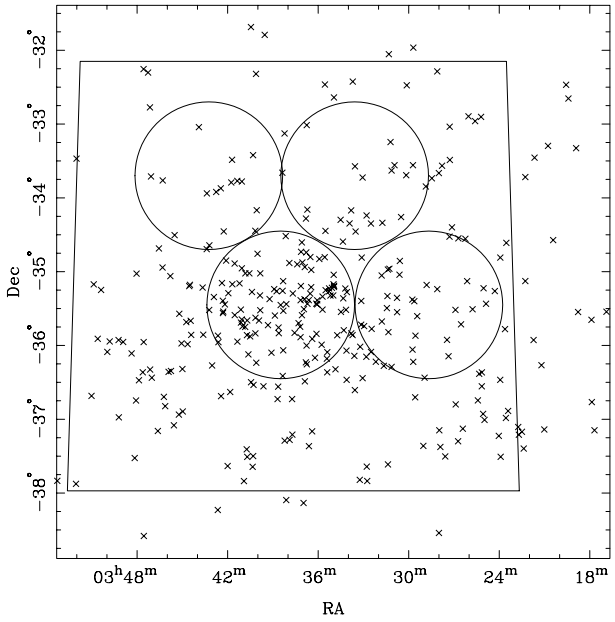

Fig. 1. Distribution of the 2dF fields observed on the sky. The crosses indicate the positions of the 340 members listed in the Fornax Cluster Catalog (Ferguson 1989). The large trapezium shows the boundary of the region imaged on the Schmidt plate.

2.3. Target selection

In common with the large 2dF Galaxy Redshift Survey (Colless 1999), we have chosen to select our targets from catalogues based on UKST Sky Survey plates digitised by the Automatic Plate Measuring facility (APM) at Cambridge. Unlike most galaxy surveys however, which only select resolved images for spectroscopic measurement, we avoid any morphological selection and include all objects, both resolved and unresolved (i.e. 'stars' and 'galaxies'). This means that we can include galaxies with the greatest possible range in surface brightnesses (and with a range of scale sizes): our only selection criterion is a (blue) magnitude limit. Including objects normally classified as stars greatly increases the size of our sample but it is the only way to ensure completeness.

Our input catalogue for the FSS is a standard APM 'catalogues' file (see Irwin et al. 1994) of field F358 from the UK Schmidt southern sky survey. The field is centred at $03^{\rm h}37^{\rm m}55.^{\rm s}9$, $-34^{\rm o}50'14''$ (J2000) and the region scanned for the catalogue file is $5.8\,\mathrm{deg} \times 5.8\,\mathrm{deg}$. This field is approximately centered on the Fornax Cluster and is slightly smaller than the region surveyed by Ferguson (1989) shown in Fig. 1. The APM image catalogue lists image positions, magnitudes and morphological classifications (as 'star', 'galaxy', 'noise', or 'merged') measured from both the blue (b_j) and red survey plates. The 'merged' image classification indicates two overlapping images: at the magnitudes of interest for this project the merged objects nearly always consisted of a star overlapping a much fainter galaxy. All the positions are measured from the more recent red survey plate (epoch 1991 September 13 compared to 1976 November 18 for the blue plate) to minimise problems with proper motions. The APM catalogue magnitudes are calibrated for unresolved (stellar) objects only, so we supplemented these with total magnitudes for the galaxies measured by direct analysis of the plate data (see Sect. 2.4).

Our target selection consisted simply of taking all objects from the APM catalogue in each of our four 2dF fields with magnitudes in the range $16.5 \leq b_j \leq 19.7$. We did not apply any morphological selection, although the APM image classifications from the blue survey plate were used to determine which photometry to use (see Sect. 2.4). The limits were chosen to avoid very bright objects which could not be observed efficiently with 2dF and for which the photographic photometry would be unreliable, whilst, at the faint end, to allow us to measure a significant area of the cluster (12 deg^2) in a reasonable amount of time. With these limits our sample contains some 14,000 objects, i.e. around 3,500 in each 2dF area. Thus each region requires a total of ten 2dF set ups (to allow for 'sky' and broken fibres).

The selection of our targets is illustrated in Fig. 2, a magnitude-surface brightness (SB) diagram of all objects in our central 2dF field ('Field 1') from the APM data. The APM points include stars which follow a well-defined locus at the bottom right of the distribution. The selection limit on the input APM catalogue (an area of 16 pixels at the isophotal detection threshold) does not impinge on the area from which our spectroscopic targets are chosen, running above the area shown in Fig. 2, at $\mathrm{SB} > 25\, b_j\,\mathrm{mag\,arcsec}^{-2}$, except for a tiny intersection with the top right hand corner of the plotted region at $b_j \simeq 20$ (i.e. our objects are well within the completeness limit of the over-

Table 2. Target numbers in Field 1 with $16.5 \leq b_j \leq 19.7$

unresolved	resolved	merged	total
2152	785	307	3244

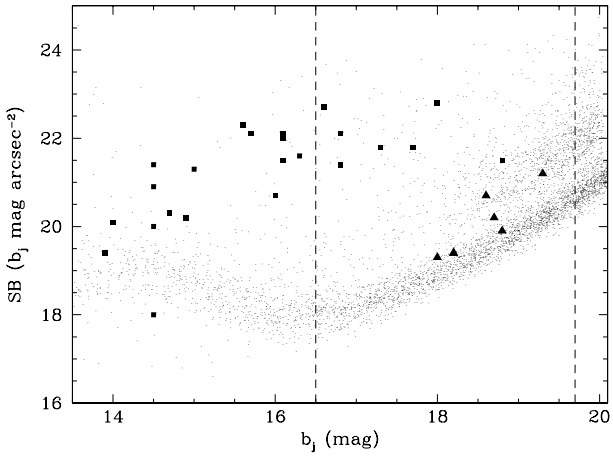

Fig. 2. Plot of central surface brightness (SB) against b_j magnitude for all objects in our APM input catalogue for the central 2dF field (points). The unresolved objects form a locus at the lower right; the surface brightness (which is optimised for galaxies and faint images) is very poor for the unresolved sources at bright magnitudes. Objects with published redshifts are indicated by solid symbols: galaxies (squares) and quasars (triangles). The two vertical dashed lines indicate the magnitude limits of our survey. The selection limit for the input APM catalogue crosses the plotted region only in the very top right hand corner at $b_j \simeq 20$, SB $\simeq 25\, b_j$ mag arcsec^{-2}.

all APM catalogue). We also show on the diagram the positions of the objects discussed above with published redshifts in this same field (very bright cluster galaxies with $b_j < 13$ were not matched). Apart from a few QSOs, the previously observed galaxies occupy a very small part of the diagram, tending to bright magnitudes and 'normal' surface brightness. Our new survey sample defined by the dashed lines includes the full range of surface brightness detected in the Schmidt data in that magnitude range. The breakdown of the sample by image classification is given in Table 2; as expected it is dominated by unresolved objects (stars).

Our final spectroscopic sample will inevitably suffer from incompleteness at the low surface brightness limit. It will not be possible to measure spectra for the faintest LSB galaxies in reasonable exposure times even though the multiplex advantage of 2dF will enable us to go much fainter than previous work.

2.4. Photometric calibration

The photometric calibration of the input catalogues is complicated by the non-linear response of the photographic emulsion. The methods we use to estimate the true fluxes are described in this section. We use different methods to measure the stars, which are often heavily saturated, to the galaxies which are mostly unsaturated. The choice of estimator is based on the automated APM classifications of the objects as 'stellar' or 'resolved', although we emphasise again that objects of all morphological types are observed. In all of the discussion below we use the photographic blue b_j magnitude defined by the IIIaJ emulsion combined with a GG 395 filter. This is related to the standard Cousins B magnitude by $b_j = B - 0.28 \times (B - V)$ (Blair & Gilmore 1982).

Table 3. Photometric calibration

Source	Type	N	meanΔ	σ_Δ	medianΔ
CCD	stars	72	0.00	0.13	0.00
Caldwell	galaxies	23	0.26	0.30	0.30
CCD	galaxies	502	-0.05	0.47	-0.14
FCC	galaxies	2033	0.24	0.52	0.20

Note: $\Delta = b_j - b_{j,calibration}$

2.4.1. Unresolved objects ('stars')

It is relatively easy to estimate the magnitudes of unresolved objects (probably stars) from photographic data because the images all have the same shape. This means that the total magnitudes can be reliably derived from the outer, unsaturated regions of the brighter objects. The object magnitudes in the APM catalogue data (Irwin et al. 1994) were measured this way using an internal self-calibration procedure to fit stellar profiles, correcting for the non-linear response of the photographic emulsion (see Bunclark & Irwin 1984). The same method was used for objects classified as 'merged', since, as discussed above, these are dominated by stars.

The default APM calibration uses a quadratic relation to convert from raw instrumental magnitudes to calibrated b_j magnitudes. We checked this calibration with CCD data and made a small adjustment to the default values. We based our recalibration on 2 stars from the Guide Star Photometric Catalog (Lasker et al. 1988), 2 fainter stars from CCD frames taken for the same project (Lasker, private communication, 1997) and 68 stars from our own CCD observations with the CTIO[2] Curtis Schmidt Telescope. In each case the photographic b_j magnitudes were derived from the BV calibration data. Our adjustment to the default APM calibration was equivalent to a shift of about 0.2 mag in the sense that our recalibrated values are fainter. We plot the calibrated CCD magnitudes against our final adopted magnitudes in Fig. 3. Our fit is very good with an r.m.s. scatter of 0.13 mag over a range of 8 magnitudes (see Table 3).

2.4.2. Resolved objects ('galaxies')

For resolved objects (probably galaxies) we did not use the APM catalogue magnitudes, but instead used total magnitudes estimated by fitting exponential disk profiles to the APM image

[2] Cerro Tololo Interamerican Observatory (CTIO) is operated by the Association of Universities for Research in Astronomy Inc. (AURA), under a cooperative agreement with the National Science Foundation as part of the National Optical Astronomy Observatories.

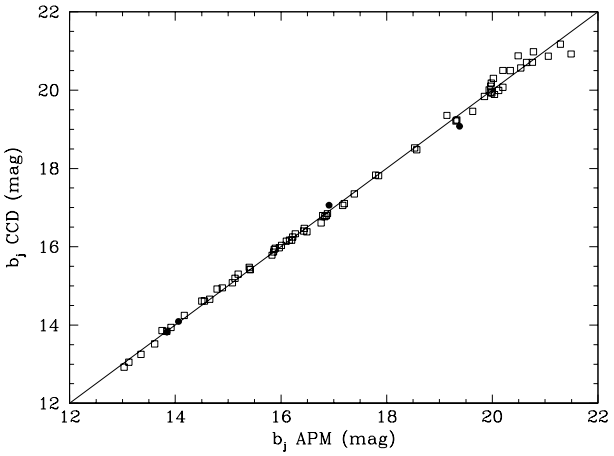

Fig. 3. Photometric b_j calibration of unresolved objects: calibrated CCD magnitudes are plotted against our recalibrated APM magnitudes for Guide Star objects (solid circles) and our new CCD observations (open squares). The line represents the identity relation between the two values.

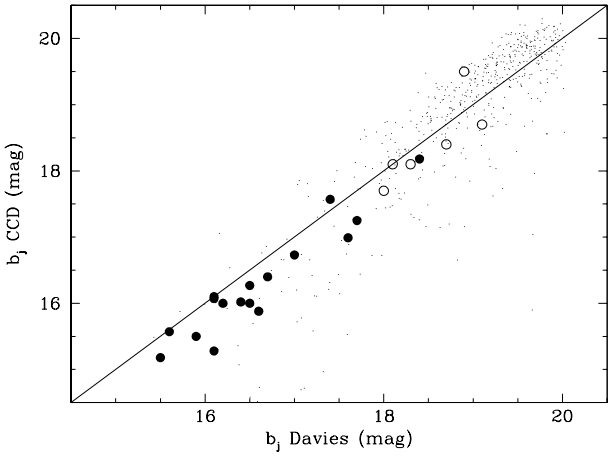

Fig. 4. Photometric b_j calibration of resolved objects: calibrated CCD magnitudes are plotted against our fitted photographic magnitudes (Davies et al. 1988) for galaxies measured by Caldwell & Bothun (1987) (solid circles; open circles indicate galaxies for which we assumed $B-V=0.72$) and our new CCD observations (points). The line represents the identity relation between the two values.

parameters (as in Davies et al. 1988 and Irwin et al. 1990). In this section we describe the calibration of these total galaxy magnitudes.

The absolute calibration was taken from the original calibration of the Fornax Schmidt survey plate by Cawson et al. (1987). They used CCD images of 18 cluster galaxies which they compared pixel by pixel with the APM machine scan data of the same galaxies. The CCD images were calibrated using standard stars and should correspond closely to the standard Johnson B band. Cawson et al. quote a calibration error of 0.1 mag.

The Cawson et al. calibration was subsequently used by Davies et al. (1988) for their sample of Fornax LSBGs and for the photometry of brighter galaxies by Disney et al. (1990). Ferguson (1989) carried out an independent calibration of galaxies in the Fornax region and where his sample overlaps with that of Davies et al. the mean difference between the two magnitude scales is 0.09 mag. The APM images data for objects classified as 'galaxies' were calibrated directly from the Davies et al. (1988) sample (see Morshidi-Esslinger et al. 1999).

At high surface brightness levels (brighter than 22.7 b_j mag arcsec^{-2}; Cawson et al. 1987; Davies et al. 1988) the limited dynamic range of the APM machine affects the calculated APM magnitude, even for galaxies. To alleviate this problem, for each galaxy we have fitted an exponential to the surface brightness profile in the range between $\mu_B = 22.7\,b_j$ mag arcsec^{-2} and the limiting surface brightness (detection isophote) $\mu_L = 25.7\,b_j$ mag arcsec^{-2}. This procedure largely overcomes the problems of saturation at the centre of an image, but of course will not allow for any central excess light such as a nucleus. We chose to use an exponential to fit each surface brightness profile because a large fraction of the galaxy population is well fitted by such a function (Davies et al. 1988). The exponential fit gives values for the extrapolated central surface brightness μ_x and the exponential scale length α. From these the relation $m_{tot} = \mu_x - 5\log(\alpha) - 1.995$ can be used to derive the total apparent magnitude m_{tot} under the fitted profile. The surface brightness profile data are supplied as part of the APM images file. (In fact, the image area at different surface brightnesses is supplied, and this is used to produce a surface brightness profile assuming circular isophotes; see Phillipps et al. 1987; Morshidi-Esslinger et al. 1999).

We compare our galaxy photometry with the CCD photometry of Caldwell & Bothun (1987) in Fig. 4. Here we have plotted total b_j magnitudes from Caldwell & Bothun against our photographic galaxy magnitudes. Following Ferguson & Sandage (1988) we have assumed $B-V=0.72$ when converting to b_j if the colour was not measured by Caldwell & Bothun. Over the whole range shown there is an average offset of about 0.2 mag in the sense that our magnitudes are fainter. We found a similar offset when comparing our whole sample to that of Ferguson (1989), also measured from photographic plates (not plotted, but listed in Table 3). We also estimated total (Kron) galaxy magnitudes using our own CCD data for a larger sample of faint galaxies: these show a small average offset in the opposite sense (see Table 3). When plotted in Fig. 4 these data give the impression that the slope of the calibration is steeper than unity, but this is also consistent with a constant offset in the Caldwell & Bothun data points as they are all at brighter magnitudes. We have retained the Davies et al. (1988) calibration without any further adjustment since we do not expect a closer agreement from methods which use different data and fit different profiles to estimate total galaxy magnitudes.

2.5. Astrometric calibration and guide stars

The input target lists (including guide stars) must have relative positions accurate to 0.3 arcsec or better over the full two degree field of the 2dF spectrograph as discussed above. This condition

is not satisfied by all image catalogues based on UKST plates—see Drinkwater et al. (1995) for a discussion of the problems. We therefore checked the accuracy of the APM positions by comparison with the Positions and Proper Motions star catalogue (PPM; Röser et al. 1994).

A total of 232 PPM stars matched stars in the APM catalogue file for the whole UK Schmidt field F358 with b_j magnitudes of 8.9–12.1. We eliminated outliers (total position errors more than 1.5 arcsec) and selected a test sample of the faintest 60 remaining stars. The mean and r.m.s. errors were (-0.39 ± 0.30) arcsec in RA and (-0.12 ± 0.23) arcsec in Dec. These errors are for the whole 6 degree field of the UK Schmidt: in a single 2dF field the scatter is about 0.25 arcsec in each direction. We also calculated the radial errors as a function of radius from the plate centre as in Drinkwater et al. (1995) to test for any overall scale errors. We found a very small error: the faint stars were slightly too far from the centre (0.089 arcsec/degree) and the bright stars were slightly too close to the centre (-0.021 arcsec/degree). This is in the same sense as we found for the COSMOS/UKST catalogue, but smaller in magnitude: there we measured 0.14 and -0.29 arcsec/degree respectively. This shift (the 'magnitude' effect) between the bright and faint stars is caused by asymmetric halos around the brighter stars which displace their image centroids away from the plate centre. The largest scale error we found would not be significant over a two-degree field, so we have established that APM catalogue positions are accurate enough for 2dF observing.

The guide stars used to align the telescope during 2dF observations must have positions to the same accuracy as the targets and—importantly—in the same reference frame. We chose stars from the same APM catalogue file as our targets but took care to minimise errors that could arise from proper motion or the 'magnitude effect'. Both these problems are reduced by selecting faint guide stars, but we can further reduce the chance of selecting stars with significant proper motions by choosing stars with blue colours and APM positions measured from the more recent red survey plates (see Drinkwater et al. 1996). We used faint blue stars with $15.5 \leq b_j \leq 16.5$ and $B - R < 1.8$. As a rule-of-thumb, this corresponds to stars with barely discernible diffraction spikes on the blue survey plates and no diffraction spikes on the red survey plates. We found that stars selected according to these criteria were easily detected by the 2dF guiding system and had consistent positions.

3. Scientific rationale

As emphasised in the Introduction, the FSS will cover all possible types of objects visible within our target magnitude range. As such, it will be useful for a large number of individual survey projects. In this section we summarise some of these, divided according to object type.

3.1. Cluster galaxies

The prime reason for choosing the sky area we have was, of course, the presence of the Fornax Cluster of galaxies. The Fornax and Virgo galaxy clusters are the nearest reasonably rich clusters (Fornax is approximately Abell Richness Class 0 – it is supplementary cluster S0373 in Abell et al. 1989). We take the distance to Fornax to be 15.4 Mpc (a distance modulus of 30.9 mag) as derived by Bureau et al. (1996), so our 2dF sample reaches absolute magnitudes around $M_B = -11$. The Fornax Cluster has been the subject of several previous spectroscopic (Jones & Jones 1980; Drinkwater & Gregg 1998; Hilker et al. 1999) and photometric studies (Phillipps et al. 1987; Davies et al. 1988; Ferguson 1989; Ferguson & Sandage 1988; Irwin et al. 1990; Morshidi-Eslinger et al. 1999).

The main motivation for an all-object survey is, of course, to determine cluster membership for a complete sample of objects (including, especially, dwarf galaxies), irrespective of morphology. This will allow us to test whether the usual assignment of LSBGs to the cluster and high (or even 'normal') surface brightness faint galaxies to the background is justified (see, for example, the contrasting views expressed in Ferguson & Sandage 1988, and Irwin et al. 1990) and enable us to determine the complete surface brightness distribution (and the joint surface brightness - magnitude distribution) for a cluster for the first time (see Phillipps et al. 1987; Phillipps 1997). We report elsewhere on the identification of a population of low luminosity, very compact HSBGs in the cluster (Drinkwater et al. 2000b = Paper IV).

3.2. Normal field galaxies

Our galaxy sample will, though, be dominated by very large numbers of background galaxies. These will be roughly 10 times more numerous than the cluster members (depending on the relative slopes of the field number counts and the faint end of the cluster luminosity function) and can obviously be used to determine a field luminosity function (LF), using the conventional approach which requires redshift data. Although containing many fewer galaxies than the major 2dF or Sloan surveys, an LF determined from the FSS sample will have the advantage of including all galaxies, irrespective of morphology, at both the high and low surface brightness ends (down, obviously, to the surface brightness limit of the 2dF observations). Surface brightness limitations on the determination of LFs have been discussed by Phillipps & Driver (1995) and Dalcanton (1998). Extending this, we will be able to determine the bivariate brightness distribution for field galaxies (i.e. the joint distribution in luminosity and surface brightness; Phillipps & Disney 1986; van der Kruit 1987; Boyce & Phillipps 1995; de Jong 1996).

3.3. Compact and LSB field galaxies

We have already detected a number of very compact field galaxies beyond the Fornax Cluster (see Paper II for details). These objects are so compact that they have been classified as 'stars' from the blue sky survey plates and therefore represent a class of galaxy missed in previous galaxy surveys based on photographic survey plates. We estimate that they represent $2.8 \pm 1.6\%$ of all galaxies in the magnitude range $16.5 \leq b_j \leq 19.7$. They are lu-

minous (within a few magnitudes of M_*) and most have strong emission lines and small sizes typical of luminous HII galaxies and compact narrow emission line galaxies. Four of the thirteen have red colours and early-type spectra, so are of a type unlikely to have been detected in any previous surveys.

Similarly we have been able to obtain spectra for a number of LSBGs beyond Fornax. Some are likely to have been misclassified as cluster members on morphological grounds (Ferguson 1989) and can only be revealed as larger background LSBGs (potential 'Malin 1 cousins'; Freeman 1999) via redshift measurements (Drinkwater et al. 1999b; Jones et al. 2000 = Paper III, in preparation).

3.4. Galactic stars

Although initially motivated by extragalactic interests, the FSS can also make significant contributions to Galactic astronomy. The lion's share of the unresolved targets in the survey will be ordinary Galactic stars, making up about 70% of the objects in the overall survey. For instance, the final tabulation will include many thousand M dwarfs in the Galactic disk. While the FSS 2dF velocity precision (~ 50 km s^{-1}) is low compared to that used in most kinematic studies of the Galaxy (e.g. Norris 1994), the sheer numbers of M dwarfs should allow a good determination of their scale height and velocity dispersion, for example. As Fornax is only $\sim 30^{\rm o}$ from the South Galactic Pole, many of the stars in the survey will belong to the halo. Although only a minor mass component of the Galaxy, the properties of the halo provide clues to the formation of the whole Milky Way. Blue horizontal branch stars from the metal poor halo will make up perhaps ~ 1% of our sample and are straightforward to recognise spectroscopically.

3.5. Radio sources

The region of our FSS is covered by two sensitive radio continuum surveys – the NRAO VLA Sky Survey (NVSS; Condon et al. 1998) and the Sydney University Molonglo Sky Survey (SUMSS; Bock et al. 1999). These cover different frequencies (1.4 GHz for NVSS, 843 MHz for SUMSS), both with an angular resolution of about 45 arcsec. The faintest radio sources catalogued by these surveys are roughly 2.5 mJy for NVSS and 5 mJy for SUMSS. At these faint flux density levels we expect to detect three main kinds of radio sources: QSOs, active galaxies and star-forming galaxies (Kron et al. 1985; Condon 1984; see also Condon 1992). The fraction of star-forming galaxies increases rapidly below 10 mJy, and below 1 mJy they become the dominant radio–source population Our 2dF spectra should discriminate reliably between AGN and starburst galaxies.

3.6. Quasi-stellar objects

As well as the foregoing radio quasars, the survey will detect one of the largest ever completely unbiased samples of optical QSOs. All previous optical QSO surveys have relied on one or more specific selection criteria, such as UV-excess or variability, to pre-select 'candidate' QSOs for follow-up spectroscopy (e.g. Boyle et al. 1991). The FSS on the other hand will be limited only by the strength of the QSO's emission lines. Preliminary results suggest that this technique detects some 10% more QSOs to the same magnitude limit as conventional multi-colour work (see Meyer et al. 2000 = Paper V).

4. Spectroscopic observations

In this section we describe our spectroscopic data from the 2dF. We give a brief summary of the observing setup and initial data reduction and then explain the semi-automated analysis we perform to classify all the spectra. Finally we present some example spectra from our initial observations.

4.1. Observing setup

We observed all our targets with the same observing setup for 2dF: the 300B grating and a central wavelength setting of 5800Å giving a wavelength coverage of 3600–8010Å at a resolution of 9Å (a dispersion of 4.3Å per pixel). This is the same setup as for the 2dF galaxy (Folkes et al. 1999) and QSO (Boyle et al. 1997) redshift surveys. We did not attempt to flux-calibrate our spectra given the difficulty of flux-calibration in fibre-fed spectroscopy, and because our objective was to measure velocities for as many objects as possible in the available time.

In order to maximise our observing efficiency we grouped our targets by their central surface brightness, so that we could vary exposure times to obtain similar quality spectra over a large range of apparent surface brightness. The exposure times ranged from 30 minutes for bright stars to four hours for LSB galaxies. Our early runs in commissioning time were limited to minimum exposures of about 2 hours and also included a range of objects and surface brightnesses, so produced some very high signal-to-noise stellar spectra. We discuss the quality of the spectra as a function of exposure time and surface brightness in Sect. 4.4.

4.2. Data reduction

The 2dF facility includes its own data reduction package (2DFDR) which permits fast, semi-automatic reduction of data direct from the instrument. When we started the project 2DFDR was still under development, so we chose instead to reduce the data with the DOFIBERS package in IRAF[3]. We are now reducing the data in parallel with 2DFDR to compare our results.

The data reduction with IRAF follows the standard procedures for multi-object fibre spectroscopy supplemented by several scripts used to reformat the image header data and tabulate the object identifications using the output from the 2dF configuration software and the 2dF fibre-spectrum lookup table.

Accurate sky-subtraction with fibre spectra is difficult and problematic (Barden et al. 1993; Watson et al. 1998) especially for the stronger night sky-lines and when the fibres are closely

[3] IRAF is distributed by the National Optical Astronomy Observatories, operated by the Association of Universities for Research in Astronomy, Inc. under cooperative agreement with the NSF.

Table 4. Templates

Name	Type	Velocity (km s^{-1})
HD 221741	A3 V	75
Hz 948	F3 V	105
SAO 57199	F6 V	170
HD 28099	G0 V	110
HD 22193	G6 V	140
SAO 76803	K5 V	95
HD 260655	M0 V	-8
BD 63 0137	M1 V	410
Yale 1755	M5 V	57
Emission Line	galaxy	0
LBQS QSO	QSO	0

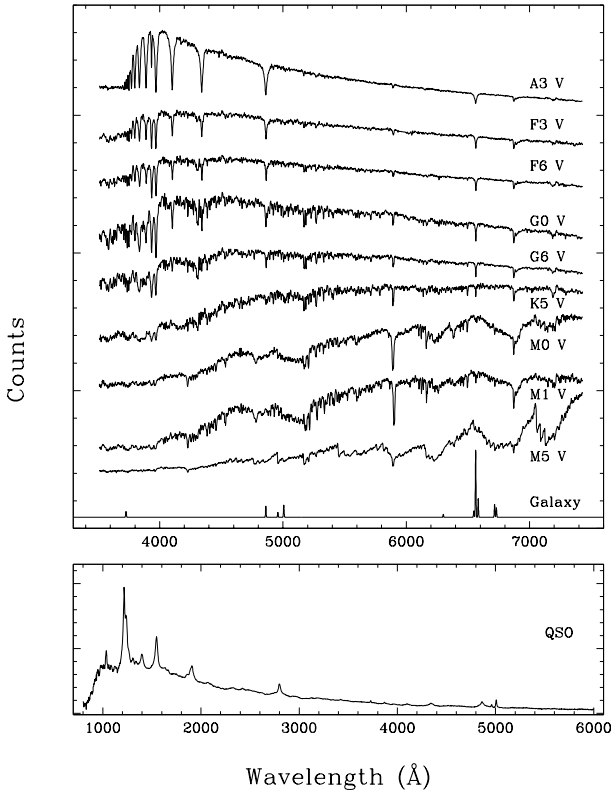

Fig. 5. Spectra of the various templates used for automatic classification and redshift estimation. See Table 4 for details.

spaced with profiles only 2-3 pixels wide (as with 2dF). After extracting the spectra we removed residuals from the strong night sky lines at 5577 and 6300Å by interpolation across the lines. The spectra were then visually inspected and any strong features due to cosmic ray events removed: these were identified by having widths less than the instrumental resolution.

We also remove atmospheric absorption features from the spectra using a simple self-calibration method. We take all the galaxies observed with a given CCD on a given night and average them with no weighting. The galaxy features cancel out as they are all at different redshifts, leaving a combination of the instrumental response and the main atmospheric absorption bands. We then fit and normalise by a continuum. Then we edit the resulting spectrum by hand to set it to unity in all regions except the main atmospheric bands at 6800–7600Å. We then divide all object spectra by this to remove the bands. This has the effect of removing the atmospheric features, but otherwise leaving the spectra unchanged with instrumental response intact. The same approach could not be used when most of the spectra on a given CCD are stars with many common features all at the same wavelengths. For these we found that a normalisation spectrum generated from galaxies observed the same night was more than adequate.

4.3. Spectral analysis

The aim of our spectral analysis is to determine a redshift and identification for all spectra ranging from Galactic stars to high redshift QSOs. In keeping with our survey philosophy we analyse all the spectra in an identical fashion, irrespective of their image morphology. To do this successfully we have adapted the usual procedure in galaxy surveys of cross-correlating against template galaxy spectra by using a set of stellar templates instead of the normal templates of absorption-line galaxies. This was previously used on a small sample of unresolved objects by Colless et al. (1993).

The first stage of the identification is to calculate cross-correlations automatically using the IRAF add-on package RVSAO (Kurtz & Mink 1998). For each spectrum-template combination this measures the Tonry & Davis (1979) R coefficient, the redshift and its error. Emission lines are not removed before performing the correlations, but the spectra are Fourier-filtered. At this stage the full available wavelength range is used for the cross-correlations. The redshifts are measured as radial velocities in units of cz and are subsequently converted to heliocentric values. By chosing the template giving the best R coefficient we can determine not only the redshift, but a first estimate of the object type. We only accept identifications with $R \geq 3$ (corresponding, in principle, to a peak in the cross-correlation which is significant at the 3 sigma level) and in addition make a check by eye for misidentifications (see below). This is straightforward for $R \geq 3$, since in practice such spectra always have three or more identifiable features. Objects with redshifts of $\approx 500\,\mathrm{km\,s^{-1}}$ or less are Galactic stars for which the best template indicates the stellar spectral type. At higher redshifts, external galaxies are separated into absorption-line types if they match one of the stellar spectra or emission-line types if they match the emission-line galaxy template best. We found that all the absorption-line galaxies that would have been detected by galaxy templates were easily measured using the stellar templates, so we do not need to use specific absorption-line galaxy templates.

The template spectra used are listed in Table 4 and plotted in Fig. 5: we use a set of nine stellar templates from the Jacoby et al. (1984) library and a synthetic emission-line galaxy spectrum provided with the RVSAO package. We constructed a second emission-line template similar to the first but limited to wave-

lengths less than 6000Å. This was needed to give reasonable fits to the high-redshift galaxies where the Hα line was shifted out of the 2dF bandpass, but strong Hβ/OIII features were present. The stellar templates were chosen to give a reasonable range of spectral types, but not more than could be separated with our low-resolution unfluxed spectra. We also note that the Jacoby et al. spectra have not been shifted to zero redshift: we therefore estimated their redshifts using a combination of individual line measurements and cross-correlation with other standards. These were then entered in the image headers to give the correct results with RVSAO; they are also listed in Table 4.

In the second stage of the identification process we check each identification interactively using the RVSAO package to display the best cross-correlation and a plot of the object spectrum with common spectral features plotted at the corresponding redshift. When the redshift is obviously wrong (e.g. with the Calcium H & K lines clearly present but misidentified), it is flagged as being wrong or in some cases is recalculated. The recaculation most commonly involves repeating the template cross-correlation on a restricted wavelength range chosen to avoid the red end of the spectrum affected by poorly removed sky features. In extreme cases the object may be a QSO: these are distinguished by strong broad emission lines and are measured using a composite QSO spectrum (Francis et al. 1991). Objects still not identified at this stage are flagged to be reobserved.

A third, supplementary stage is used for any spectra measured with good signal (a signal-to-noise ratio $>$10 in each 4.3Å wide pixel) but no obvious features in their 2dF spectra: these are flagged as 'strange' and scheduled for detailed follow-up observations with conventional slit spectrographs.

Once the spectroscopic redshift measurements are complete, they are corrected to heliocentric values. We checked the accuracy of the redshift measurements by comparing the results for 66 objects with repeated measurements. The r.m.s. scatter of the velocity differences is $90\,\mathrm{km\,s^{-1}}$. This uncertainty is consistent with the combined error estimates for the same measurements produced by RVSAO: the mean predicted error was $92\,\mathrm{km\,s^{-1}}$. Note that this implies a measurement error of a single observation of $90/\sqrt{2} \simeq 64$ km s^{-1}. We also compared our results to redshifts of 44 galaxies found in a search of the literature using NED (most were from Hilker et al. 1999). The comparison gave a mean velocity difference of (7 ± 17) km s^{-1} and an r.m.s. scatter of 111 km s^{-1}, entirely consistent with our internal calibration.

The 2dF spectra, although of low resolution and unfluxed, are useful for more detailed analysis than simple redshift measurements and object classifications (c.f. Tresse et al. 1999). We defer any detailed analysis of the spectra to later papers dealing with specific object classes, but note here that, even for the lowest luminosity galaxies, they can be used to measure emission line equivalent widths, and hence star formation rates, line widths (limited by the resolution of 900 km s^{-1}), emission line ratios (e.g. OIII/Hβ and NII/Hα), absorption line indices (e.g. CaIIH+Hϵ/CaIIK and Hδ/FeI4045) and even ages and metallicities from these Balmer and the metal absorption lines (Paper II; Folkes et al. 1999).

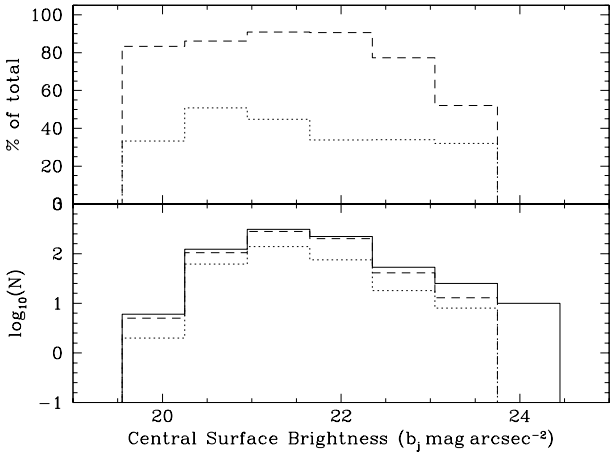

Fig. 6. The number of galaxies (resolved objects) observed which have successful redshift measurements as a function of surface brightness. The lower panel shows the total number of galaxies observed (solid line), the number with measured redshifts (dashed line) and the number of those which have strong emission lines (dotted). The upper panel again shows the successfully measured (dashed) and emission line (dotted) galaxies, this time as a fraction of those observed.

4.4. Current status

Although this present paper is mainly concerned with the principles behind the FSS, we already have a considerable amount of 2dF data for the project from commissioning observations in 1996/1997, and scheduled time in December 1997/January 1998 and November 1998. We have nearly completed our observations of the first field having observed 92% of all targets in the range $b_j = 16.5$ to 19.7 and successfully obtained redshifts for 94% of those observed.

For resolved objects (galaxies) the success rate of our redshift measurements is a function of surface brightness. In Fig. 6 we plot the numbers of galaxies observed and identified as a function of central surface brightness. We have attempted to optimise the exposure times to the surface brightnesses of the objects, using exposures up to 3.75 hours for the lower surface brightness images. The identification rate runs at 78% or better to a limit of $23\,b_j$ mag arcsec^{-2}. Fainter than this limit (corresponding to a mean surface brightness inside the detection threshold $\sim 24.5\,b_j$ mag arcsec^{-2}), the identifications drop off rapidly. The unresolved objects at higher surface brightness (mostly stars) have an identification rate of 95% in our target magnitude range of $b_j = 16.5$ to 19.7.

In Fig. 7 we show example spectra from our initial observations of the various types of object discussed above. The first two spectra are Galactic stars, an M-dwarf and a white dwarf. The next two spectra are of normal low-redshift galaxies, one with an absorption line spectrum and one with an emission line spectrum. The remaining four spectra are all of objects that were unresolved (i.e. classified as stars in the target catalogues), but have been identified as various types of galaxy. The first is a compact emission line galaxy (CELG; see Sect. 3.3), the second is a normal, optically selected QSO and the third is an X-ray source. The final spectrum is of a fainter radio-loud quasar.

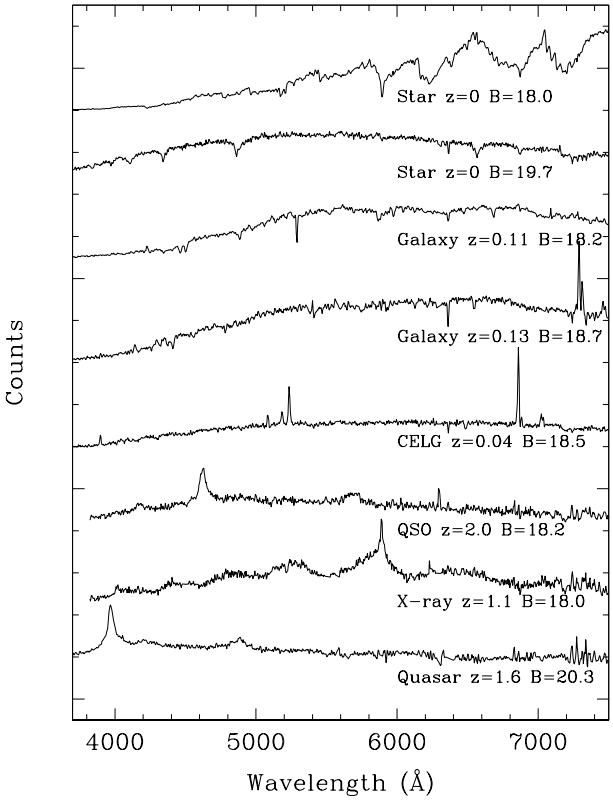

Fig. 7. Example spectra of stars, galaxies and quasars from our initial 2dF observations. See text for a brief description of the spectra.

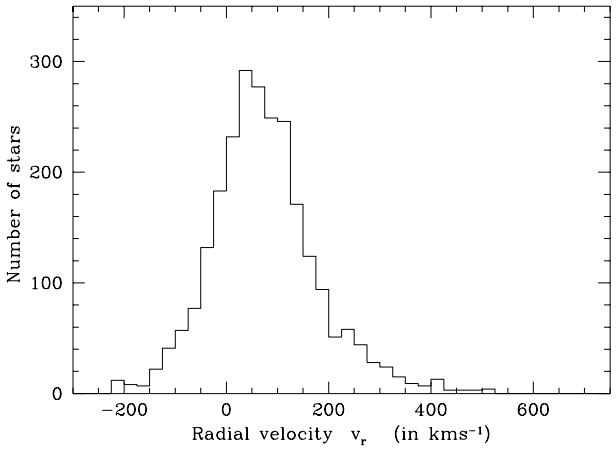

Fig. 8. The heliocentric radial velocity distribution for Galactic stars.

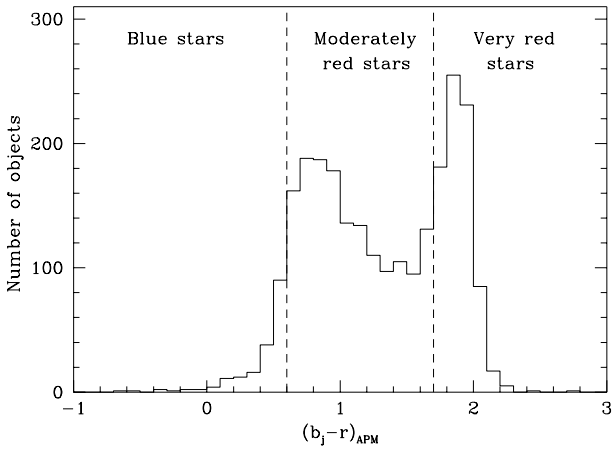

Fig. 9. The colour distribution for Galactic stars. The histogram shows the distribution of the $(b_j - r)_{\rm APM}$ colour index for the stars of FSS Field 1 having reliable velocities. The colour limits of the subsamples of stars are indicated by dashed lines.

5. Initial scientific results: velocity distributions from the first 2dF field

The number of galaxies observed in the Fornax Cluster itself is not yet large enough to allow a detailed study of the cluster population: this will require results from the remaining three 2dF spectrograph fields to achieve the statistical samples needed. However, we have ample data to delineate clearly the velocity structure in the direction of Fornax. In particular, we have determined accurately the velocity distribution of Galactic stars, as well as the galaxy distribution in redshift space behind the cluster.

5.1. Radial velocities of Galactic stars

The radial velocity distribution of Galactic stars is revealed in the existing FSS results, despite the modest resolution of the spectra compared to those conventionally used in kinematic surveys of the Galaxy. A total of 2467 objects in Field 1 of Table 1 have reliable radial velocities $v_r < 750$ km s^{-1}. The estimated standard errors in the velocities are typically $\pm 25 - 80$ km s^{-1}, sufficiently small to reveal the contributions of different Galactic components.

Fig. 8 shows the distribution of all FSS Field 1 objects with reliable ($R \geq 3$) velocities less than $750\,{\rm km\,s^{-1}}$. The field has Galactic co-ordinates $(l, b) = (237^{\rm o}, -54^{\rm o})$, so we are sampling a sight-line looking diagonally 'down' through the Galactic plane between the anti-centre and anti-rotation directions. The component of the motion of the local standard of rest in this direction is $-120\,{\rm km\,s^{-1}}$. For our chosen magnitude range, the survey will sample predominantly disc, thick disc and halo main sequence stars, with some contribution from halo giants and disc white dwarfs (Gilmore & Reid 1983). The results can be compared with dedicated spectroscopic studies of faint stars in high-latitude fields (e.g. Kuijken & Gilmore 1989; Croswell et al. 1991; Majewski 1992).

The contribution of the various Galactic components can be demonstrated by considering subsamples of the stars defined by colour. Basic colour information can be derived from the blue and red magnitudes given in the APM Catalogue. Fig. 9 shows the distribution of these $(b_j - r)_{\rm APM}$ colours for the Field 1 objects with velocities $v_r \leq 750\,{\rm km\,s^{-1}}$. The form of the distribution is similar to that obtained in dedicated studies of the properties of faint stars (e.g. Reid & Majewski 1993). We divide the stars into three samples: relatively blue stars having $(b_j - r)_{\rm APM} \leq 0.6$; moderately red stars having $0.6 < (b_j - r)_{\rm APM} \leq 1.7$; and very red stars having $(b_j - r)_{APM} > 1.7$.

The sharp decline in numbers bluewards of $(b_j - r)_{\rm APM} \simeq 0.6$ is the result of the main sequence cut-off for moderately old stellar populations; the blue sample extends to this limit. These limits at $(b_j - r) = 0.6$ and 1.7 correspond to $(\rm B - V) \simeq 0.4$ and 1.1

The moderately red stars are expected to include G and K dwarfs in the thick disc and halo, G and K giants in the halo, and disc K dwarfs. The halo component, being dynamically pressure supported, has a broad radial velocity distribution which is displaced relative to the solar motion by the component of the solar rotation velocity towards Fornax (Freeman 1987; Gilmore, Wyse & Kuiken 1989; Majewski 1993). Disc and thick disc stars, being rotationally supported, have a zero or small asymmetric drift and a modest intrinsic velocity dispersion: their velocity distributions will be centred closer to zero heliocentric velocity. The moderately-red star sample is therefore expected to have a broad velocity distribution with the halo component contributing a high velocity tail, consistent with the velocity distributions shown in Fig. 10. In contrast, the very red star sample will be rich in disc late K and M dwarfs and will include halo late K and M giants. It is therefore expected to have only a modest net drift with respect to the local standard of rest but with a tail to high velocity, as observed in Fig. 10. The blue stars include local (disc) white dwarfs and halo horizontal branch stars. They are therefore expected to have a broad range of velocities, consistent with the results here.

Of particular interest is the high velocity tail at $v_r \geq 400$ km s^{-1}. If the extreme examples are confirmed by higher resolution spectroscopy they will provide useful constraints on the mass of the Galaxy (e.g. Carney et al. 1988; Croswell et al. 1991; Majewski et al. 1996; Freeman 1999, private communication).

5.2. Galaxies in the foreground of the Fornax Cluster

A gap is present in the velocity distribution between the cut-off in Galactic stars at $cz \simeq 550$ km s^{-1} and the Fornax Cluster at $cz \simeq 900 - 2200$ km s^{-1}. No objects are found in this intermediate velocity range among the results from the first 2dF field. The low velocity limit of the cluster velocity distribution is therefore defined without ambiguity.

It is of interest to determine whether there are any galaxies in the foreground to the Fornax Cluster having heliocentric radial velocities $cz < 600$kms^{-1} which might be overlooked given the very large number of Galactic stars in this velocity range. The APM Catalogue (used as the input database for the survey) provides a classification for each image from the blue and red sky survey plates. Of the 2467 objects having $cz < 600$ km s^{-1} and cross-correlation R parameter ≥ 3.0, 14 are classified as being galaxies in both blue and red. All 14 were inspected visually on the Digitised Sky Survey and again on a SuperCOSMOS measuring machine (Miller et al. 1992) scan of film OR17818 taken on Tech Pan emulsion with the UKST. The Tech Pan data provided higher resolution and greater depth than the Digitised Sky Survey (e.g. Phillipps & Parker 1993). All foreground galaxy candidates appeared to be compact images merged with another, fainter image. Most were unambiguously Galactic stars merged with either another star or with a background galaxy. None of the 14 candidates had the extended appearance expected of a nearby dwarf galaxy.

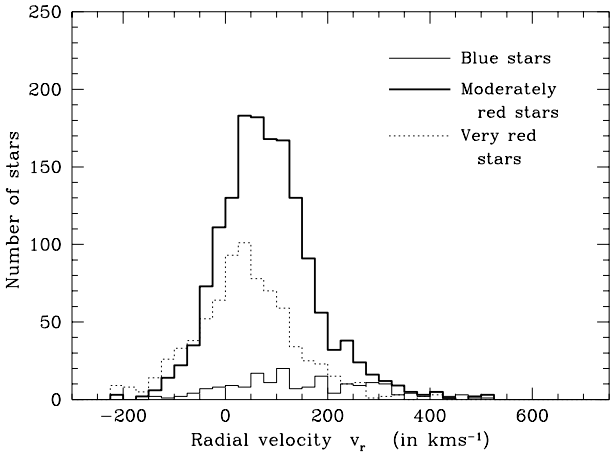

Fig. 10. The radial velocity distribution for Galactic stars segregated by colour. As Fig. 8 but showing the heliocentric radial velocities distinguished according to the APM $(b_j - r)$ colour index. The stars are divided into blue ($(b_j - r)_{\rm APM} \leq 0.6$), moderately red ($0.6 < (b_j - r)_{\rm APM} \leq 1.7$) and very red ($(b_j - r)_{\rm APM} > 1.7$) samples.

To extend the search, the visual inspection was repeated on the five images with reliable velocities ≤ 600 km s^{-1} having the largest APM σ parameter on the blue sky survey plates. The σ parameter measures the degree to which an image differs from a point-spread function and is a convenient indicator of a non-stellar light profile. Of the five images having a blue $\sigma_{\rm B} > 38.0$, none had the appearance expected of a nearby dwarf galaxy: all were found to be compact (star-like) images merged with either another star or a faint galaxy.

A third and final search for foreground galaxies was performed using large exponential scale lengths as a indicator of extended images. The surface photometry described in Sect. 2.4.2 derived a scale length from the low surface brightness regions of each image. Only five images with reliable velocities ≤ 600 km s^{-1} had scale lengths $\alpha > 1.5$ arcsec. None had the appearance expected of a nearby dwarf galaxy on the Digitised Sky Survey or the scan of the Tech Pan film: all objects were again found to be merged images. We conclude that no foreground galaxies were found with star-like velocities.

We therefore have no galaxies with heliocentric $cz < 900$ km s^{-1} in Field 1 of Table 1 within our magnitude range. Among the brighter galaxies ($B < 16$) in the whole cluster region, Jones & Jones (1980) previously found a small number with such low velocities (NGC 1375, NGC 1386, NGC 1396 ($\equiv$ G75), and NGC 1437A), though the exact number depends on the accuracy of their redshift determinations. A search of the *NASA Extragalactic Database* (*NED*) identifies the same four galaxies. Of these, NGC 1375, NGC 1386 and NGC 1396 lie in our Field 1.

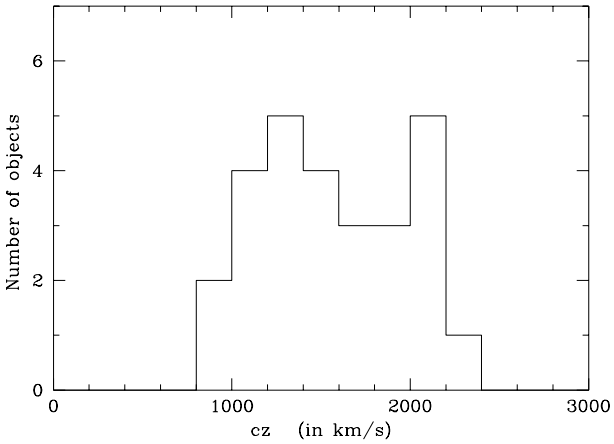

Fig. 11. The heliocentric radial velocity distribution of Fornax Cluster galaxies from the *FSS* in Field 1. Objects with velocities < 600 km s^{-1} (Galactic stars) are not shown for the sake of clarity.

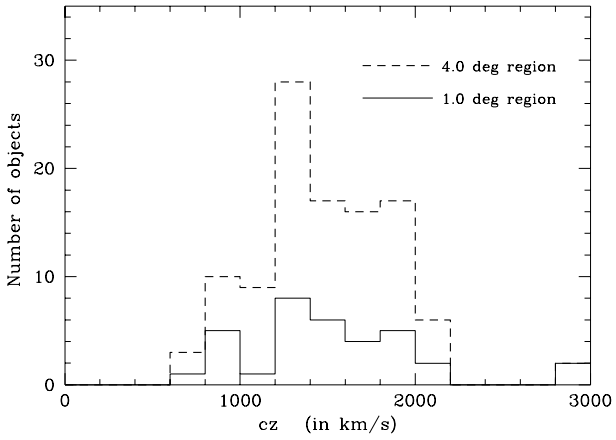

Fig. 12. The heliocentric radial velocity distribution of Fornax Cluster galaxies compiled from the *NASA Extragalactic Database* within *FSS* Field 1 (solid histogram) and within a 4.0-degree radius region centred on the field (dashed histogram). The area of the 4.0-degree radius region is, of course, 16 times that of Field 1.

5.3. The velocity structure of the Fornax Cluster

Fig. 11 shows the velocity distribution of Fornax Cluster galaxies from the FSS. The mean heliocentric radial velocity from the FSS data is 1560 ± 80 km s^{-1} (26 galaxies). This compares with 1540 ± 50 km s^{-1} from Jones & Jones. Recall that the Jones & Jones galaxies are much brighter than ours (roughly $-21 \leq M_{\rm B} \leq -15$ as against $-14 \leq M_{\rm B} \leq -11$) and are spread over a much larger area, 6 degrees or about 1.6 Mpc across compared to our 2 degrees or 0.5 Mpc. A velocity dispersion can be estimated fairly unambiguously as there are no galaxies with velocities less than 900 or between 2300 and 3000 km s^{-1}. Our 26 galaxies give an observed radial velocity dispersion of 380 ± 50 km s^{-1}, compared to the 391 km s^{-1} of Jones & Jones.

The FSS velocity distribution can also be compared with the equivalent distribution compiled from all published redshift data. Fig. 12 presents the velocity data from *NED*. These give a mean heliocentric radial velocity of 1450 ± 70 km s^{-1} (32 galaxies), and a velocity dispersion of 370 ± 50 km s^{-1}, entirely consistent with the *FSS* results. The *NED* results generally, though not entirely, apply to the brighter cluster galaxies.

Fornax is an apparently well relaxed, regular cluster as judged by its central density concentration and low spiral content. It would require a very much larger sample of redshifts over the other fields in order to explore properly any dynamical differences between different galaxy populations. These initial results do not reveal any difference in the dynamics between the bright and faint (giant and dwarf) members of the cluster, although a wide-field study of brighter galaxies (Drinkwater et al. 2000a) does suggest such a difference.

5.4. The velocity structure behind the Fornax Cluster

Fig. 13 shows our redshift distribution behind the cluster. Immediately beyond the cluster, as noted by Jones & Jones (1980) and Phillipps & Davies (1992), there is a large void, extending some 40 Mpc (from the cluster mean redshift to about 5000 km s^{-1} assuming $H_0 = 75$ km s^{-1} Mpc^{-1}). Beyond this "Fornax Void", we see the ubiquitous 'spiky' distribution (Broadhurst et al. 1990) showing more distant walls and filaments.

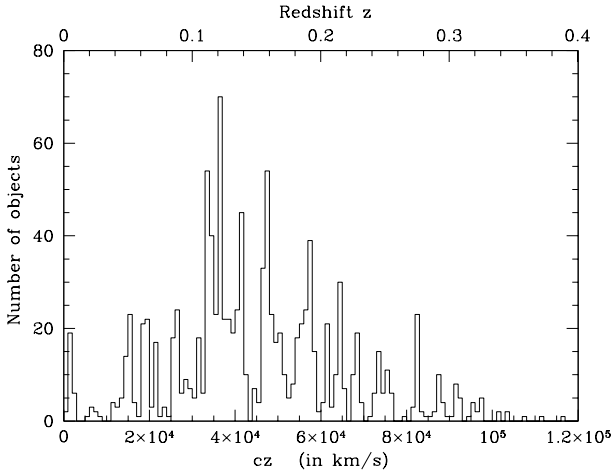

Fig. 13. The radial velocity distribution from the *FSS* in Field 1 showing the population behind the Fornax Cluster. Objects with velocities $<$ 600 km s^{-1} (Galactic stars) are not shown for clarity.

Fig. 14 shows the distribution of background galaxies taken from the *NED*. The difference in depth between the two data sets is immediately apparent: the FSS results probe to much greater distances on account of the fainter magnitudes of the galaxies. Nevertheless, the first two main features in our distribution clearly match the two peaks seen in the *NED* data (i.e. in the brighter galaxies).

A standard cone diagram is shown in Fig. 15, illustrating the skeleton of the large scale 3-D structure beyond Fornax. The median redshift of the entire galaxy sample is 0.15. This compares with a mean of 0.11 in the preliminary data from the 2dF Galaxy Redshift Survey (Colless 1999). The data continue to map structure out to $z \simeq 0.30$, where there are still significant numbers of galaxies. The cluster J1556.15BL identified by

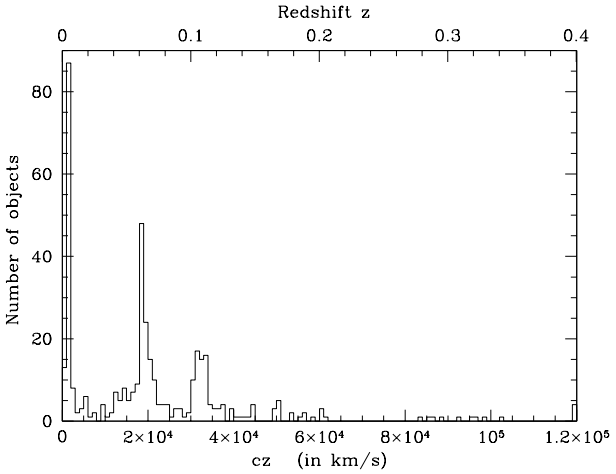

Fig. 14. The radial velocity distribution from the *NASA Extragalactic Database* showing the population behind the Fornax Cluster. The figure shows all galaxies found in the *NED* within a 4.0 deg radius region centred on *FSS* Field 1.

Couch et al. (1991) lies in Field 1 at $z = 0.457$, but the density of FSS galaxies at this redshift is too small to show the cluster.

In addition to the general galaxy population, Fig. 15 also shows (as large solid points) the compact galaxies discussed in Paper II. These objects have star-like images on Schmidt survey plates but the 2dF spectroscopy showed them to be compact star-forming galaxies at redshifts $0.04 - 0.21$. The figure also shows low surface brightness galaxies having intrinsic (cosmologically corrected) central surface brightnesses fainter than $22.5\ b_j$ mag arcsec^{-2}, plotted as open circles. Despite their low surface brightnesses, these objects are sufficiently distant that they are too luminous to be dwarfs given the apparent magnitude limits of the survey (they have $M_{\rm B} \simeq -17$ to -19 for $H_0 = 75$ km s^{-1} Mpc^{-1}).

Many authors (e.g. Phillipps & Shanks 1987; Eder et al. 1989; Thuan et al. 1991; Loveday et al. 1995; Mo et al. 1994) have discussed whether or not low luminosity and/or low surface brightness galaxies follow the same structures as the brighter component. Although, as stated earlier, this sample is not yet complete – so we can not use strictly objective measures such as the galaxy correlation function (Phillipps & Shanks 1987) – we do have enough information in our distribution to see that the low surface brightness galaxies (shown as open circles in Figs. 16 and 15) do trace the same large scale structure and are not seen "filling the voids"(Dekel & Silk 1986). The present data extend this comparison of the distribution of LSBG with that of normal galaxies to significantly lower surface brightnesses than most other studies (or, indeed, will be possible with the standard SLOAN or GRS samples). Similarly, the compact (high surface brightness) galaxies, which are also likely to be missing from other surveys, again follow the same overall large scale structure in Fig. 15 as the general galaxy population. This is unlike the suggestions from some previous emission line galaxy surveys (e.g. Salzer 1989) that such objects can appear in very low density regions.

6. Summary

In this paper we have presented an overview of the FSS, the first complete, all-object spectroscopic survey to cover a large area of sky. This project has only been made possible by the advent of the 400-fibre Two-degree Field spectrograph on the Anglo-Australian Telescope. In total we hope to observe some 14,000 objects to a magnitude limit of b_j=19.7 — both 'stars' and 'galaxies' — in a 12 square degree area of sky centred on the Fornax Cluster.

The main technical challenges of the project concern the preparation of the target catalogue and the analysis of the resulting spectra. Our input catalogues are based on UK Schmidt Sky Survey plates digitised by the APM facility. We have demonstrated that the APM image catalogues provide sufficiently accurate target positions and photometry for the unresolved sources. For the resolved sources our photometry is derived by fitting exponential profiles to the image parameters measured by the APM. We have tested our calibration with new CCD observations. We use a semi-automated procedure to classify our spectra and measure radial velocities based on cross-correlation comparison with a set of stellar spectra, two emission-line galaxy spectra and one QSO spectrum. This procedure successfully identifies stars, galaxies and QSOs completely independently of their image morphology.

When the FSS is complete we will have a unique, complete, sample of Galactic stars, Fornax Cluster galaxies, field galaxies and distant AGN. We have discussed some of the scientific questions that can be addressed with such a sample. The principal objective is to obtain an unbiased sample of cluster members, which includes compact galaxies and low surface brightness dwarfs, independent of a membership classification based on morphological appearance.

Redshift/velocity distributions are presented here based on spectroscopic results from the first of four 2dF fields. The velocity distribution of Galactic stars can be understood in terms of a conventional three-component model of the Galaxy. The Fornax Cluster dwarf galaxies in the first 2dF field have a mean heliocentric radial velocity of 1560 ± 80 km s^{-1} and a radial velocity dispersion of 380 ± 50 km s^{-1}. The Fornax Cluster is well-defined dynamically, with a low density of galaxies in the foreground and immediate background. Beyond 5000 km s^{-1}, the large-scale structure behind the Fornax Cluster is clearly delineated out to a redshift $z \simeq 0.30$. The compact galaxies found behind the cluster by Drinkwater et al. (1999a) are found to follow the structures delineated by the general galaxy population, as are background low surface brightness galaxies. Some more detailed initial results have already been presented elsewhere (Drinkwater et al. 1999a, 1999b).

Acknowledgements. This project would not be possible without the superb 2dF facility provided by the AAO and the generous allocations of observing time we have received from PATT and ATAC. MJD is grateful for travel support from the University of Bristol and the International Astronomical Union. SP acknowledges the support of the Royal Society via a University Research Fellowship. JBJ and JHD are supported by the UK PPARC. SP, JBJ and RMS acknowledge the

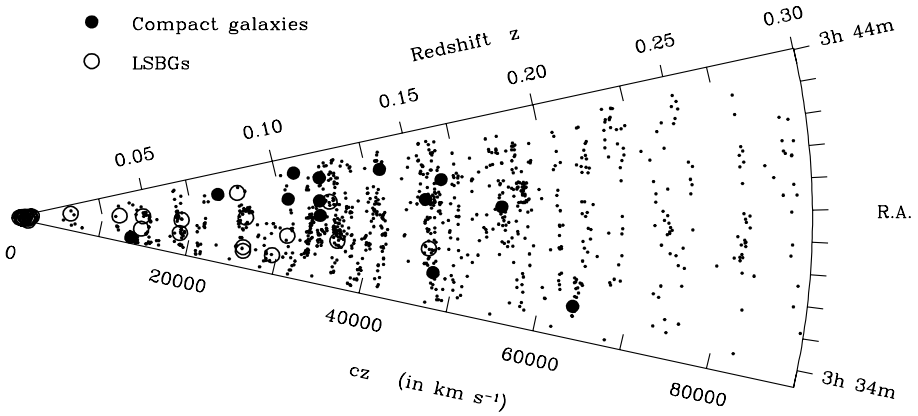

Fig. 15. The radial velocity distribution of the galaxies behind the Fornax Cluster from Field 1 of the *FSS* as a function of J2000 right ascension showing the distribution of low surface brightness and compact galaxies. LSBGs, having intrinsic central surface brightnesses $> 22.5\ b_j$ mag arcsec^{-2}, are shown as open circles. The compact galaxies of Drinkwater et al. (1999a, Paper II) are shown as filled circles. Note that the right ascension axis has been greatly expanded (by a factor of 12.5 times) for clarity (falsely giving the peaks in the galaxy density the appearance of shells).

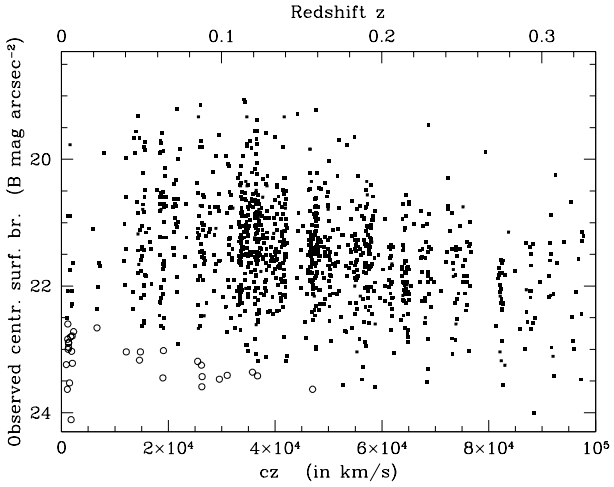

Fig. 16. The central surface brightness of the *FSS* sample plotted against redshift. The blue surface brightnesses are taken from the surface photometry described in Sect. 2.4.2. Low surface brightness galaxies, having intrinsic central surface brightnesses $> 22.5\ b_j$ mag arcsec^{-2}, are plotted as open circles. The conversion from observed to intrinsic surface brightnesses uses cosmological surface brightness dimming and k-corrections from Coleman et al. (1980).

hospitality of the School of Physics, University of New South Wales. Part of this work was done at the Institute of Geophysics and Planetary Physics, under the auspices of the U.S. Department of Energy by Lawrence Livermore National Laboratory under contract No. W-7405-Eng-48. We would also like to thank the referee, Dr Jon Loveday, for constructive comments on the original version of this paper.

References

Abell G.O., Corwin H.G. Jr., Olowin R.P., 1989, ApJS 70, 1
Barden S.C., Elston R., Armandroff T., Pryor C.P., 1993, In: Gray P.M. (ed.) Fiber Optics in Astronomy II, ASP Conf. Ser. 37, p. 223
Blair M., Gilmore G., 1982, PASP 94, 742
Bock D., Large M.I., Sadler E.M., 1999, AJ, in press, astro-ph/9812083
Bothun G.D., Impey C.D., Malin D.F., Mould J.R., 1987, AJ 94, 23
Boyce P.J., Phillipps S., 1995, A&A 296, 26
Boyle B.J., Jones L.R., Shanks T., 1991, MNRAS 251, 482
Boyle B.J., Smith R.J., Shanks T., et al., 1997, In: Sato K. (ed.) Cosmological Parameters and Evolution of the Universe. Proc. IAU Symp. 183, p. 6
Broadhurst T.J., Ellis R.S., Koo D.C., Szalay A.S., 1990, Nat 343, 726
Bunclark P., Irwin M.J., 1984, In: Capaccioli M. (ed.) Astronomy with Schmidt-type Telescopes. Proc. IAU Colloq. 78, Reidel, Dordrecht, p. 147
Bureau M., Mould J.R., Staveley-Smith L., 1996, ApJ 463, 60
Caldwell N., Bothun G.D., 1987, AJ 94, 1126
Carney B.W., Latham D.W., Laird J.B., 1988, AJ 96, 560
Cawson M.G.M., Kibblewhite E.J., Disney M.J., Phillipps S., 1987, MNRAS 224, 557
Coleman G.D., Wu C.-C., Weedman D.W. 1980, ApJS 43, 393
Colless M.M., 1999, Phil. Trans. R. Soc. London, Ser. A 357, 105
Colless M.M., Ellis R.S., Broadhurst T.J., Taylor K., Peterson B.A., 1993, MNRAS 261, 19
Condon J.J., 1984, ApJ 287, 461
Condon J.J., 1992, ARA&A 30, 55
Condon J.J., Cotton W.D., Greisen E.R., et al., 1998, AJ 115, 1693
Couch W.J., Ellis R.S., Malin D.F., MacLaren I., 1991, MNRAS 249, 606
Croswell K., Latham D.W., Carney B.W., Schuster W.J., Aguilar L., 1991, AJ 101, 2078
Dalcanton J.J., 1998, ApJ 495, 251
Davies J.I., Phillipps S., Cawson M.G.M., Disney M.J., Kibblewhite E.J., 1988, MNRAS 232, 239
Dekel A., Silk J., 1986, ApJ 303, 39
Disney M.J., Phillipps S., Davies J.I., Cawson M.G.M., Kibblewhite E.J., 1990, MNRAS 245, 175
Drinkwater M.J., Barnes D.G., Ellison S.L., 1995, PASA 12, 248
Drinkwater M.J., Barot J., Irwin M., 1996, In: The Anglo-Australian Observatory Newsletter No. 79, p. 7
Drinkwater M.J., Gregg M.D., 1998, MNRAS 296, L15
Drinkwater M.J., Gregg M.D., Holman B.A., Brown M., 2000a, MNRAS, submitted
Drinkwater M.J., Gregg M.D., Jones J.B., Phillipps S., 2000b, PASA, submitted (Paper IV)
Drinkwater M.J., Phillipps S., Gregg M.D., et al., 1999a, ApJ 511, L97 (Paper II)
Drinkwater M.J., Phillipps S., Jones J.B., 1999b, In: Davies J.I., Impey C.D., Phillipps S. (eds.) The Low Surface Brightness Universe. Proc. IAU Colloq. 171, ASP, San Francisco, p. 120
Eder J.A., Oemler A., Schombert J.M., Dekel A., 1989, ApJ 340, 29
Ferguson H.C., 1989, AJ 98, 367 (FCC)
Ferguson H.C., Sandage A., 1988, AJ 96, 1520
Folkes S., Ronen S., Price I., et al., 1999, MNRAS 308, 459
Francis P.J., Hewett P.C., Foltz C.B., et al., 1991, ApJ 373, 465
Freeman K.C., 1987, ARA&A 25, 603

Freeman K., 1999, In: Davies J.I., Impey C.D., Phillipps S. (eds.) The Low Surface Brightness Universe. Proc. IAU Colloq. 171, ASP, San Francisco, p. 3
Gilmore G.F., Reid I.N., 1983, MNRAS 202, 1025
Gilmore G.F., Wyse R.F.G., Kuijken K., 1989, ARA&A 27, 555
Gunn J., 1995, A&AS 186, 44.05
Hilker M., Infante L., Vieira G., Kissler-Patig M., Richtler T., 1999, A&AS 134, 75
Irwin M.J., Davies J.I., Disney M.J., Phillipps S., 1990, MNRAS 245, 289
Irwin M.J., Maddox S., McMahon R., 1994, Spectrum 2, 14
Jacoby G.H., Hunter D.A., Christian C.A., 1984, ApJS 56, 257
Jones J.E., Jones B.J.T., 1980, MNRAS 191, 685
de Jong R.S., 1996, A&A 313, 45
Kron R.G., Koo D.C., Windhorst R.A., 1985, A&A 146, 38
Kuijken K., Gilmore G.F., 1989, MNRAS 239, 605
Kurtz M.J., Mink D.J., 1998, PASP 110, 934
Lasker B.M., Sturch C.R., Lopez C., et al., 1988, ApJS 68, 1
Lewis I.J., Glazebrook K., Taylor K., 1998, SPIE 3355, 828
Loveday J., Maddox S.J., Efstathiou G., Peterson B.A., 1995, ApJ 442, 457
Loveday J., Pier J., 1998, In: Colombi S., Mellier Y., Raban B. (eds.) Wide Field Surveys in Cosmology. 14th IAP Colloquium, Editions Frontières, in press, astro-ph/9809179
Majewski S.R., 1992, ApJS 78, 87
Majewski S.R., 1993, ARA&A 31, 575
Majewski S.R., Munn J.A., Hawley S.L., 1996, ApJ 459, L73
Meyer M.J., Drinkwater M.J., Phillipps S., Couch W.J., 2000, MNRAS, submitted (Paper V)
Miller L.A., Cormack W., Paterson M., Beard S., Lawrence L., 1992, In: MacGillivray H.T., Thomson E.B. (eds.) Digitised Optical Sky Surveys. Kluwer Academic Publishers, p. 133
Mo H.J., McGaugh S.S., Bothun G.D., 1994, MNRAS 267, 129
Morshidi-Esslinger Z.B., Davies J.I., Smith R.M., 1999, MNRAS 304, 297
Morton D.C., Krug P.A., Tritton K.P., 1985, MNRAS 212, 325
Norris J.E., 1994, ApJ 431, 645
Phillipps S., 1997, In: Kontizas E., Kontizas M., Morgan D.H., Vettolani G.P. (eds.) Wide-Field Spectroscopy. Kluwer Academic Publishers, p. 281
Phillipps S., Davies J.I., 1992, In: MacGillivray H.T., Thomson E.B. (eds.) Digitised Optical Sky Surveys. Kluwer Academic Publishers, p. 295
Phillipps S., Disney M.J., 1986, MNRAS 221, 1039
Phillipps S., Disney M.J., Kibblewhite E.J., Cawson M.G.M., 1987, MNRAS 229, 505
Phillipps S., Driver S.P., 1995, MNRAS 274, 832
Phillipps S., Parker Q.A., 1993, MNRAS 265, 385
Phillipps S., Shanks T., 1987, MNRAS 229, 621
Röser S., Bastian U., Kuzmin A., 1994, A&AS 105, 301
Reid N., Majewski S.R., 1993, ApJ 406, 635
Salzer J., 1989, ApJ 347, 152
Sandage A., Binggeli B., Tammann G., 1985, AJ 90, 385
Smith R.M., Driver S.P., Phillipps S., 1997, MNRAS 287, 415
Taylor K., Cannon R.D., Parker Q.A., 1998, In: McLean B.J., Golombek D.A., Hayes J.J.E., Payne H.E. (eds.) New Horizons from Multi-Wavelength Sky Surveys. Proc. IAU Symposium 179, Kluwer Academic Publishers, p. 135
Thuan T.X., Alimi J.-M., Gott J.R., Schneider S.E., 1991, ApJ 370, 25
Tonry J.L., Davis M., 1979, AJ 84, 1511
Tresse L., Maddox S., Loveday J., Singleton C., 1999, MNRAS 310, 262
van der Kruit P.C., 1987, A&A 173, 59
Watson F.G., Offer A.R., Lewis I.J., 1998, In: Arribas S., Mediavilla E., Watson F.G. (eds.) Fiber Optics in Astronomy III, ASP Conf. Ser. 152, p. 50